

# ANALYSIS OF LOAD INTERACTION EFFECT FOR WELDED DETAILS UNDER VARIABLE AMPLITUDE FATIGUE

Kentaro YAMADA<sup>1</sup>, Qiuliang CAO<sup>2</sup> and Akimasa KONDO<sup>3</sup>

<sup>1</sup> Member of JSCE, Ph.D., Professor, Dept. of Civil Eng., Nagoya University (Chikusa-ku, Nagoya 464-8603, Japan)

<sup>2</sup> Member of JSCE, Dr. of Eng., Yokogawa Techno-Information Service Inc., (Funabashi 273-0026, Chiba, Japan)

<sup>3</sup> Member of JSCE, Dr. of Eng., Professor, Dept. of Civil Eng., Meijo University (Tenpaku-ku, Nagoya 468-8502, Japan)

Influence of load interaction on fatigue behavior of highway bridge components under service loading condition is to be clarified for better understanding of variable amplitude fatigue. Fatigue crack growth analyses considering crack closure effect are carried out on non-load-carrying cruciform joints under periodic overload (POL), variable amplitude block loading (BL) and variable amplitude (VA) loading. The analytical results are compared with those of the tests carried out in the past. Crack closure effect exists in most cases, and load interaction effect is significant under POL and BL. However, load interaction effect is insignificant under VA loading.

**Key Words:** load interaction, variable amplitude loading, non-load-carrying cruciform joint

## 1. INTRODUCTION

In the current fatigue design specifications, such as BS5400<sup>1)</sup>, ECCS<sup>2)</sup>, AASHTO<sup>3)</sup> and JSSC<sup>4)</sup>, Miner's rule is normally used for the fatigue assessment under variable amplitude (VA) loading. For welded details where high welding residual stress exists, a number of studies have shown that this method can give consistent predictions for VA loading with all cycles above the constant amplitude (CA) fatigue limit. Service loading spectrum for highway bridges usually contains a large number of small stress cycles that are lower than CA fatigue limit.

The following two shortcomings of Miner's rule have been pointed out. First, Miner's rule, known as linear cumulative damage rule, does not account for effect of load sequence, such as high-low or low-high sequence. For example, in the VA fatigue test by Melhem and Klippstein<sup>5)</sup>, long-tail loading spectrum, which contained a few large stress ranges in the spectrum, was found to cause longer fatigue life than short-tail one, the spectrum of which was truncated in the large stress range region. This is the case when a few heavy trucks exist in service of highway bridges. Second, it still remains to be fully discussed how the stress cycles below CA fatigue limit affect the fatigue life.

In order to investigate the load interaction effect that occurs due to load sequence, a large number of

studies were carried out in the past two decades. The following gives a summary on those performed by the authors. At first, a series of fatigue crack growth measurements were carried out<sup>6),7),8),9),10)</sup>. Center-cracked tension (CCT) specimens were used for the experiments and the loading spectra included CA loading, single overload (SOL), periodic overload (POL), variable amplitude block loading (BL) and VA loading. For simulating the cases where low or high welding residual stress exists in a welded joint, the fatigue loads were applied under constant minimum stresses or constant maximum stresses. Then, fracture mechanics-based fatigue crack growth predictions<sup>11)</sup> were carried out for the above tests. Load interaction effect was taken into account in the computation by considering crack closure concept<sup>12)</sup>. Good agreements were found between the predicted and experimental results.

The present study aims at extending the analytical procedures to more practical problems, such as the load interaction effect on highway bridge components. Two series of fatigue tests on non-load-carrying cruciform joints were used for comparative study. One was carried out under POL and BL loading in mid 1970s<sup>13),14)</sup>, and the other one was carried out under VA loading in 1997<sup>15)</sup>. In both cases, CA fatigue tests were also used for the purpose of comparison. In spite of the success on the fatigue crack growth analysis of CCT specimens mentioned

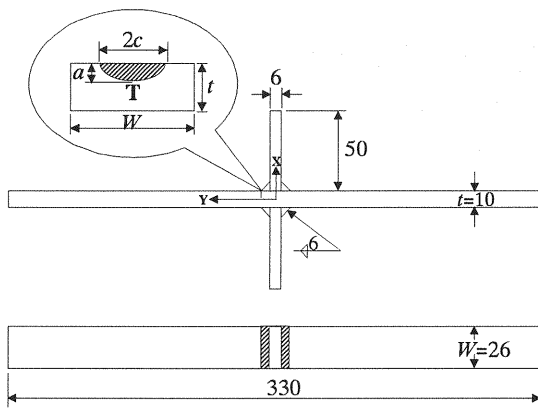


Fig. 1 Specimen tested under POL and BL loading

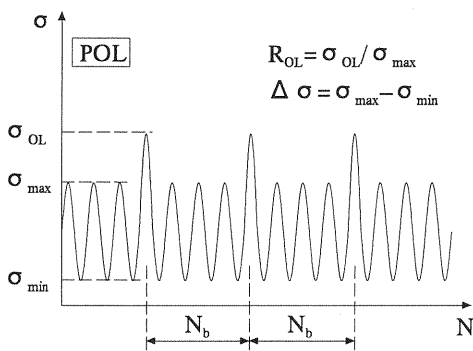


Fig. 2 POL loading spectrum

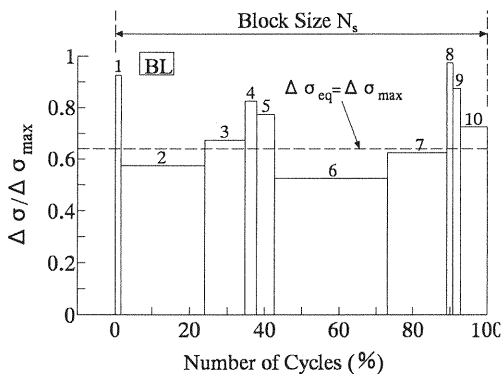


Fig. 3 BL Loading spectrum

above, the work is complicated by at least two problems for welded details. They are: (1) the consideration of welding residual stress and welding profile, and (2) the percentage of fatigue crack initiation life in total fatigue life. In the present study, assumptions are made on the distribution of welding

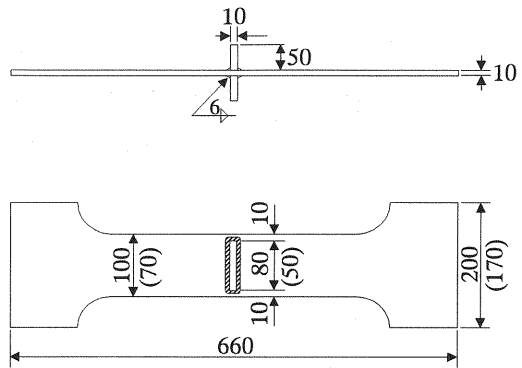


Fig. 4 Specimen tested under VA loading

residual stress and weld profile. Then fatigue crack growth analysis is carried out. Fatigue crack initiation life is obtained by subtracting the calculated fatigue crack growth life from the experimental total fatigue life.

## 2. FATIGUE TESTS TO BE ANALYZED

### (1) Fatigue tests under POL and BL loading

Two series of fatigue tests were carried out in mid 1970s for small-scale non-load-carrying cruciform joint, as shown in Fig. 1, under CA, POL and BL loading<sup>13,14</sup>. The plate material conformed to ASTM A588 for high-strength low-alloy structural steel with 345MPa minimum yield point. The measured yield point and tensile strength of the steel were 421MPa and 565MPa, respectively. Also shown in the figure is a typical semi-elliptical crack initiating from weld toe. The lengths of the minor and major semi-axes are  $a$  and  $c$ , respectively. Point T is where the minor axis intersects the crack front.

The loading spectra are shown in Figs. 2 and 3. For POL loading, the minimum stress,  $\sigma_{\min}$ , was kept at 3MPa. Three levels of stress range,  $\Delta\sigma = 144\text{MPa}$ ,  $177\text{MPa}$  and  $229\text{MPa}$ , were used. At each level, overload stress range was 1.67 times of  $\Delta\sigma$ , and the overload intervals,  $N_b$ , ranged from 10 to  $10^6$ .

For BL loading, each loading block contained 10 different loading levels. The minimum stress,  $\sigma_{\min}$ , was kept at 3MPa and the root-mean-cube (RMC) stress ranges were selected at 133MPa, 196MPa and 249MPa. The block sizes ranged from  $10^2$  to  $10^5$ .

### (2) Fatigue tests under VA loading

In order to investigate the fatigue behavior under VA loading in long life region, fatigue tests were carried out by Kondo and Yamada in 1997<sup>15</sup>. The

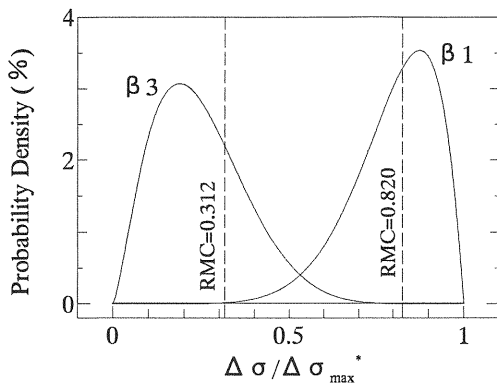


Fig. 5 Basic probability density distributions with respect to normalized stress range

non-load-carrying cruciform joints, as shown in Fig. 4, were made of structural steel SM520B. Yield point and ultimate strength were 402MPa and 539MPa, respectively.

The loading patterns,  $\beta 1$  and  $\beta 3$ , as shown in Fig. 5, were used to produce the three types of loading spectra,  $\beta 1L$ ,  $\beta 3L$  and  $\beta 3H$ . The former two had the constant minimum stress and the third one had the constant maximum stress. For comparison, CA fatigue tests were also carried out with constant minimum stress of 20MPa (A-series), constant maximum stresses of 260MPa (B-series) and 370MPa (C-series).

### 3. ANALYSIS CONSIDERING CRACK CLOSURE

The same fatigue crack growth model, as used for the analysis on the experiments of CCT specimens, is used here. This is a two-dimensional strip-yield model, in which crack closure can be considered. In order to keep the applicability of the model under relatively complicated loading spectra, e.g., POL, BL and VA loading, much effort has been made on crack-tip deforming behavior, mesh generation method, and the computation on opening stress. More information on the modeling can be found in Ref. 11.

In the present study, fatigue crack growth analysis is carried out under the experimental conditions by using the following solutions of stress intensity factor and crack opening displacement. Crack of the semi-elliptical shape is assumed to be  $a/c=1/3$  during the whole fatigue crack propagation. Initial and final crack sizes of 0.2mm and 8mm, are also assumed. These assumptions are based on the previous experimental and analytical results, such as those in

Refs. 14, 16 and 17. Such assumptions make the analysis rather simple, and allow us to compare only the interaction effect on the fatigue crack propagation. From the previous experience, the fatigue crack propagation life based on such assumptions is often between lower bound and mean fatigue life of test results, since it neglects fatigue crack initiation life.

#### (1) Solutions of stress intensity factor and crack opening displacement

In order to apply the established fatigue crack growth model, the solutions of stress intensity factor and crack opening displacement (COD) under remote uniform stress (normal stress) and partially distributed crack surface stress are necessary. Though the analytical solutions are available for CCT specimens, no solution is available for cruciform joint. For the approximate computation of the stress intensity factor under remote uniform stress, the following equation was proposed<sup>18)</sup>.

$$K_{cruciform} = F_s \cdot F_E \cdot F_T \cdot F_G \cdot \sigma_{cruciform} \sqrt{\pi a} \quad (1)$$

where  $\sigma_{cruciform}$  is the applied nominal stress and  $a$  is the crack size. Correction factors,  $F_s$ ,  $F_E$ ,  $F_T$  and  $F_G$ , accounts for the effects of free surface, elliptical crack shape, finite thickness and stress concentration, respectively, the detailed information of which can be found in Ref. 18.

For the computation of COD,  $K$ -analogy concept<sup>19)</sup> is used. In this approach, the stresses applied on the cruciform joint are transferred to those on a CCT specimen with crack size of  $2a$  and specimen width of  $2t$ , during which the stress intensity factor levels,  $K$ , are kept unchanged, i.e.,  $K_{cruciform}=K_{CCT}$ . Here,  $K_{CCT}$  can be calculated by the following equation.

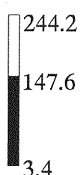
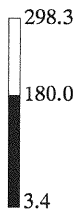
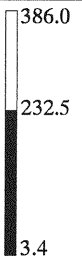
$$K_{CCT} = F_T \cdot \sigma_{CCT} \sqrt{\pi a} \quad (2)$$

Equating Eqs.(1) and (2) gives:

$$\sigma_{CCT} = F_s \cdot F_E \cdot F_G \cdot \sigma_{cruciform} \quad (3)$$

where  $\sigma_{CCT}$  is the stress applied to the CCT specimen. Once the stress transferring is finished, the computation can be carried out on the corresponding CCT specimen. It is expected that the plastic zone size, COD near the crack tip, residual plastic deformation and therefore the fatigue crack growth behavior are almost the same for these two configurations.

**Table 1** Experimental total life,  $N$ , and computed crack propagation life,  $N_p$ , for POL tests ( $\times 10^3$ )

Loading Spectrum (Stress Unit: MPa)						
	$N$	$N_p$	$N$	$N_p$	$N$	$N_p$
CA	1,862	1,041	791	587	317	288
POL10	1,035	863	350	507	151	256
POL10 <sup>2</sup>	1,801	1,005	549	591	311	299
POL10 <sup>3</sup>	1,995	1,254	1,472	715	504	360
POL10 <sup>4</sup>	>7,900	1,877	2,121	1,029	732	488
POL10 <sup>5</sup>	>10,000	1,315	2,038	690	891	321
POL10 <sup>6</sup>	No data	1,216	>4,348	645	No data	306

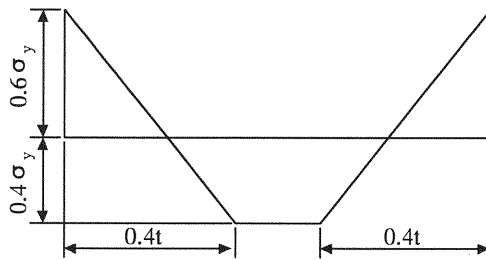


**Fig. 6** Assumed welding residual stress distribution

## (2) Closure-free fatigue crack growth equation

The mean curve of  $da/dN$  versus  $\Delta K$  relation proposed by JSSC for high tensile residual stress condition is used here as the closure-free fatigue crack growth equation, as shown in Eq. (4):

$$da/dN = C(\Delta K^m - \Delta K_{th}^m) \quad (4)$$

where  $C=1.5 \times 10^{11}$ ,  $m=2.75$ ,  $\Delta K_{th}=2.9$ . The units of  $da/dN$  and  $\Delta K$  ( $\Delta K_{th}$ ) are m/cycle and  $\text{MPa}\sqrt{\text{m}}$ , respectively.

## (3) Welding residual stress

The distribution of the transverse welding residual stress along the potential crack line is assumed for the presently discussed cruciform joint, as shown in **Fig. 6**. For simplicity, the distribution is assumed to be linear and the stresses are assumed to vary from 60% of the yield point in tension at the weld toes to 40% of the yield point in compression at the center of the

plate.

Equivalent external load approach<sup>20)</sup> is used for taking into account the influence of welding residual stress. The equivalent external load is a remote uniform stress, which results in the same stress intensity factor at the crack tip as the welding residual stress field. In the first step, stress intensity factor caused by the welding residual stress field is calculated. Then equating it and Eq.(1) gives the equivalent external load for the current crack size. Note that the stress here should be superimposed onto that applied on the cruciform joint before the  $K$ -analogy method is used for the stress transferring.

For the purpose of comparison, the computation is also carried out without residual stress for several loading cases under VA loading.

## 4. ANALYTICAL RESULTS FOR POL LOADING

### (1) Computed crack propagation life

The same POL loads as in the tests are applied in the computation until the final crack size is reached. The test data, i.e., the tested total fatigue life,  $N$ , and the computed fatigue crack propagation lives,  $N_p$ , for POL tests and corresponding CA tests are listed in **Table 1**, and are shown in **Fig. 7**. Here, stress range is the value without overloads. For comparison, the test data are also plotted.

The computed  $N_p$  are normalized with respect to the CA fatigue lives at the same stress range, as shown in **Fig. 8**. The results obtained through LEFM (Linear Elastic Fracture Mechanics) analysis, i.e.,

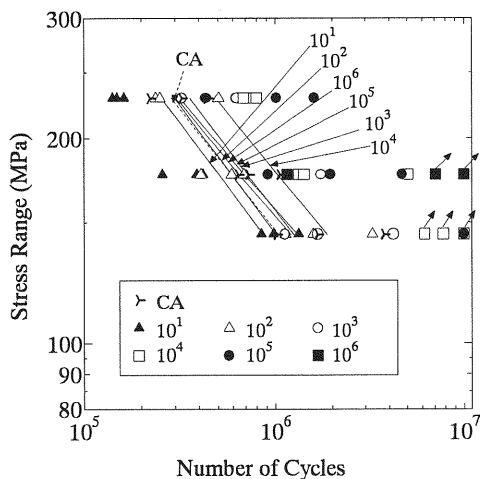


Fig. 7 Computed crack propagation life under POL loading

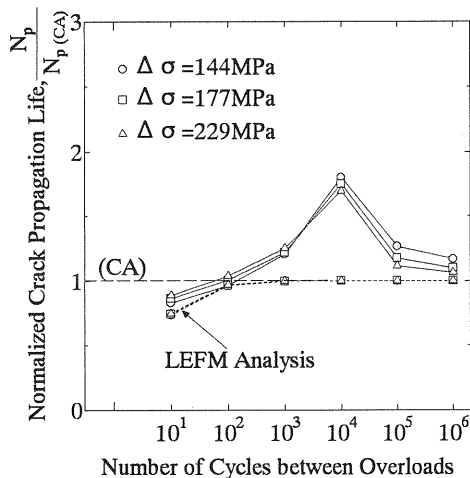


Fig. 8 Normalized crack propagation life under POL loading

without load interaction, are also shown in the figure for comparison.

Both LEFM analysis and the analysis considering crack closure show little effect of stress range on the normalized crack propagation life. The three data points at each overload interval, corresponding to three different levels of stress ranges, are quite close to each other.

For LEFM analysis, it can be seen that the normalized crack propagation lives of POL10 are lower than the corresponding value under CA loading, 1.0. This seems to result from the damage effect of the frequently applied overloads, which accelerate the fatigue crack propagation process. From POL10<sup>2</sup>, the normalized crack propagation lives under POL

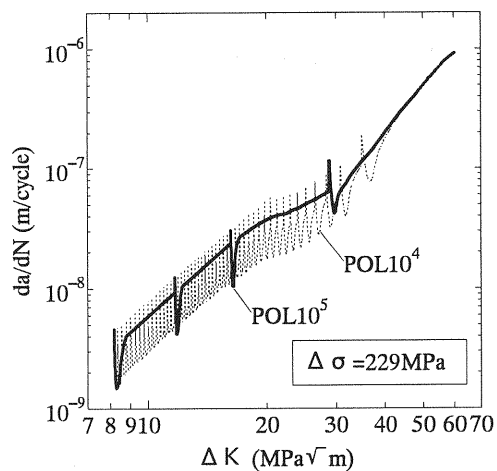


Fig. 9 Comparison between POL10<sup>5</sup> and POL10<sup>4</sup> ( $\Delta\sigma = 229\text{MPa}$ )

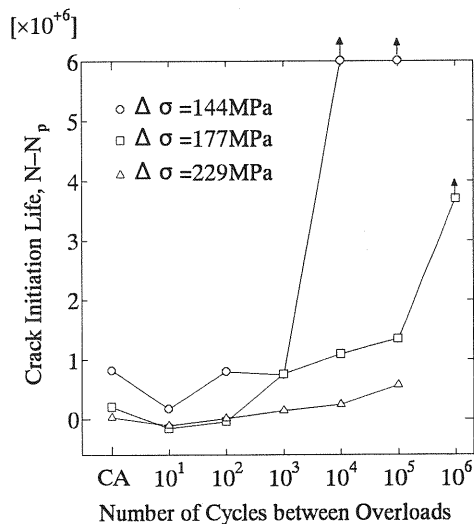


Fig. 10 Crack initiation life under POL loading

loading become close to those under CA loading.

The analysis considering crack closure makes all data points rise up to some extent when compared with LEFM analysis. This seems due to the load interaction effect that is not considered in LEFM analysis. In order to quantitatively investigate the load interaction effect, the following observations should be considered.

(a) For POL10, the normalized crack propagation life is still lower than 1.0. It means that the POL crack propagation life is shorter than that under CA loading. This indicates that the beneficial effect coming from overload-induced fatigue crack growth retardation is not large enough to compensate the corresponding damage effect.

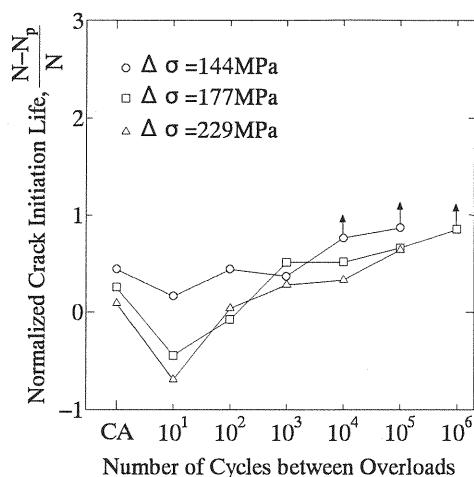


Fig. 11 Normalized crack initiation life under POL loading

- (b) With the increase in the overload interval, the normalized crack propagation life becomes larger, and it reaches the highest value, about 1.7, at  $POL10^4$ . Two mechanisms seem to contribute to this point. First, the number of overloads decreases with the increase in the overload interval. Consequently, the detrimental effect of overloads diminishes. Second, in the case of multiple overloads, the largest fatigue crack growth retardation occurs if the overload is applied just when the delaying effect of the previous one expired. The overload interval of  $10^4$  seems to be near this case. For smaller overload interval, the retardation process caused by an overload may be interrupted by the next overload before the overload effect fully activates. For  $POL10^4$ , the number of overloads is not so large, and the second mechanism occupies a dominant position.
- (c) When the overload interval increases more to  $10^5$  and  $10^6$ , the fatigue crack growth retardation effect decrease. This can be explained by the second mechanism stated above, i.e., reapplying the overload later than the critical point will reduce the fatigue crack growth retardation effect. As an example, Fig. 9 shows a comparison between  $POL10^4$  and  $POL10^5$  loading at  $\Delta\sigma = 229\text{MPa}$ . It can be seen that the crack tip is always located in the overload-affected region for  $POL10^4$ , so that the fatigue crack propagates in a low speed all the time. For  $POL10^5$ , however, the specimen experiences only four overloads during the whole crack propagation procedure. When an overload is applied, the crack tip has propagated out of the previous overload-affected region, i.e.,

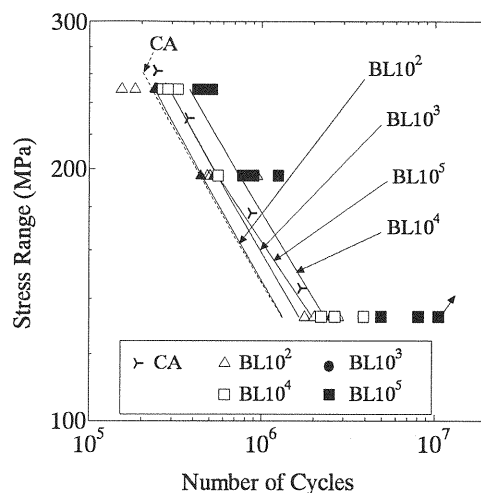


Fig. 12 Computed crack propagation life under BL loading

fatigue crack growth rate,  $da/dN$ , has recovered to the CA level. Fatigue crack growth retardation only occurs near the four overloads.

## (2) Crack initiation life

The crack initiation lives,  $N_i$ , calculated by  $N_i = N - N_p$ , are shown in Fig. 10. In Fig. 11,  $N_i$  are normalized with respect to the fatigue lives,  $N$ , obtained from the tests. What should be noted is that the data points with arrows are those with unlimited fatigue lives in the tests. No discussion will be done on their positions in the figure. The delaying effect on fatigue crack initiation is found for all of the overload intervals greater than  $10^2$ . In addition, the following two trends can be found from these two figures. First, for the same stress range, as overload interval increases, both  $N_i$  and normalized  $N_i$  also increase. Second, for the same overload interval, when the stress range becomes high, both  $N_i$  and normalized  $N_i$  decrease. The possible reasons are as follows.

- (a) As indicated by Abtahi et al.<sup>13</sup>, an overload creates residual compression stresses at the weld toe, which tends to delay the crack initiation by reducing the tensile portion of a stress cycle. This conclusion seems to be supported by the fact that most POL tests led to prolonged crack initiation life in comparison with CA test. For example, a few overloads in the test of  $POL10^6$  at  $\Delta\sigma = 177\text{MPa}$  prevented fatigue crack initiation.
- (b) As far as the influence of the number of overloads is concerned, Abtahi et al. pointed out that periodic overload application was more beneficial in delaying initiation than a single overload because the residual compressive stresses near the weld toe is reestablished

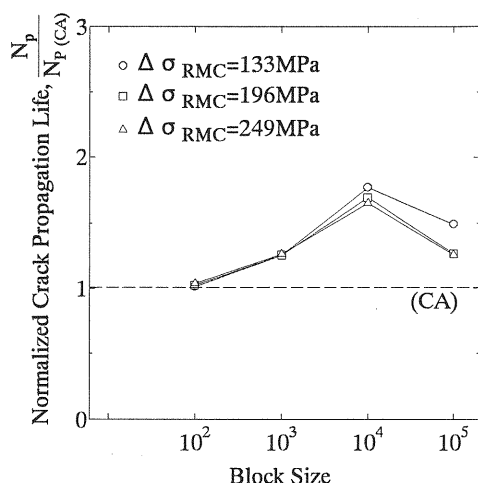


Fig. 13 Normalized crack propagation life under BL loading

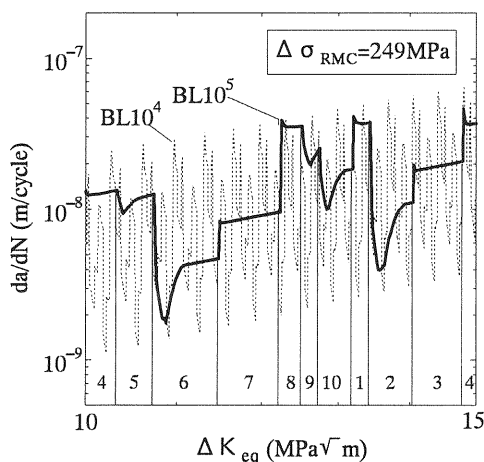


Fig. 14 Comparison between BL10<sup>5</sup> and BL10<sup>4</sup>  
( $\Delta\sigma_{RMC} = 249 \text{ MPa}$ )

whenever the overload is applied. This is demonstrated by the comparison between the test of POL10<sup>6</sup> and a single-overload test<sup>13)</sup> at  $\Delta\sigma = 177 \text{ MPa}$ . No crack initiated in the former, while the latter had finite fatigue life. The POL tests under more overloads, however, point to the contrary. As stated earlier, for the same stress range, crack initiation life tended to be shorter when the number of overloads increased. From this it is known that increasing the number of overloads is not necessarily beneficial in delaying initiation. This might result from the detrimental effect of the overloads themselves. Reminding of the fact that the limit in the frequency of overload occurrence for delaying the crack propagation process is about 10<sup>4</sup>, the corresponding value for

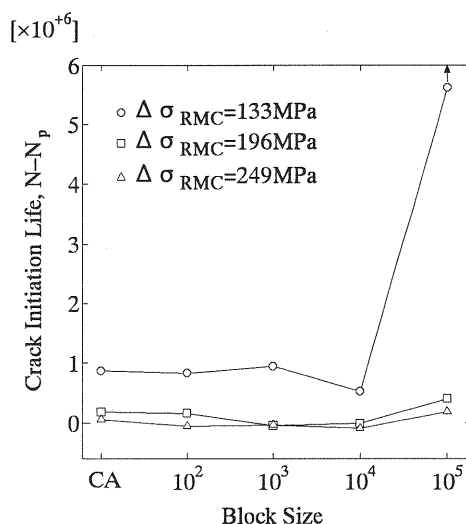


Fig. 15 Crack initiation life under BL loading

delaying the crack initiation process seems to be much smaller.

- (c) Generally, the log-log plot of  $S-N_i$  relation has relatively smaller slope than that of  $S-N_p$  relation<sup>21)</sup>, where  $S$  is the stress range. The crack propagation stage often dominates the fatigue life at high amplitude loads, while crack initiation plays a major role in long-life region. This can be used to explain why the normalized crack initiation life decreased, i.e., crack initiation life tended to occupy a reduced proportion of the total fatigue life, with the increase of the frequency of overload occurrence.
- (d) The above observation is the same as that in CA tests, i.e., with the decrease of stress range, crack initiation tends to play a more important role when compared with crack propagation.

## 5. ANALYTICAL RESULTS FOR BL LOADING

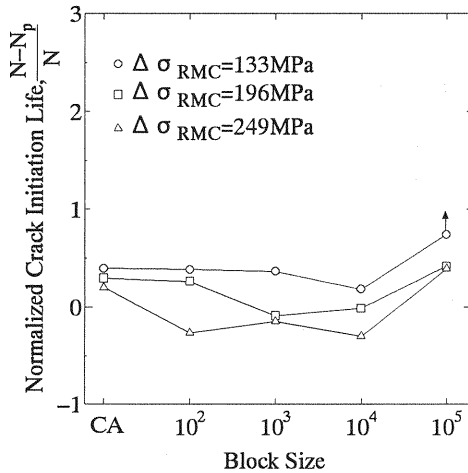
### (1) Computed crack propagation life

The test data and the computed  $N_p$  for BL loading are listed in Table 2, and are shown in Fig. 12. Here stress range is the equivalent value, i.e., the root-mean-cube value of all stress cycles in a loading block. For the same stress range, BL10<sup>2</sup> shows almost the same fatigue crack propagation life as CA. However, the  $S-N_p$  curves of the other three are higher than that of CA, which seems to be caused by the load interaction effect. The effect is the most significant for BL10<sup>4</sup>.

The computed  $N_p$  are normalized with respect to the CA fatigue lives at the same stress range, as

**Table 2** Experimental total life,  $N$ , and computed crack propagation lives,  $N_p$ , for BL tests ( $\times 10^3$ )

Loading Spectrum (Stress Unit: MPa)	$(\Delta\sigma_{RMC} = 133)$		$(\Delta\sigma_{RMC} = 196)$		$(\Delta\sigma_{RMC} = 249)$	
	$N$	$N_p$	$N$	$N_p$	$N$	$N_p$
BL10 <sup>2</sup>	2,162	1,333	612	450	189	239
BL10 <sup>3</sup>	2,595	1,653	508	553	254	290
BL10 <sup>4</sup>	2,856	2,334	736	745	292	379
BL10 <sup>5</sup>	>7,590	1,968	959	558	477	289

**Fig. 16** Normalized crack initiation life under BL loading

shown in **Fig. 13**.

The data points for BL10<sup>2</sup> almost coincide with that of CA, indicating that little crack growth retardation occurs in this case. When the block size becomes larger from 10<sup>2</sup> to 10<sup>4</sup>, the crack growth retardation effect increases gradually. However, for BL10<sup>5</sup>, the retardation effect drops down again. Therefore, the block size of 10<sup>4</sup> seems to show the largest effect in such loading cases.

**Figure 14** shows the fatigue crack growth rate,  $da/dN$ , versus the equivalent stress intensity factor range,  $\Delta K_{eq}$ , relations for BL10<sup>5</sup> and BL10<sup>4</sup> loading at  $\Delta\sigma_{RMC}=249\text{MPa}$ . In the figure, the ten loading levels in a BL10<sup>5</sup> loading block are marked by the corresponding numbers. Obviously, fatigue crack growth retardation occurs at 2, 5, 6, 9 and 10, which agrees well with the observation in the fatigue crack

**Table 3** Experimental total life,  $N$ , and computed crack propagation lives,  $N_p$ , for CA tests ( $\times 10^3$ )

Series Name	$\sigma_{min}$ (MPa)	$\Delta\sigma$ (MPa)	$N$ by experiments	$N_p$ by Closure Analysis
A	19	181	492	212
			545	
			514	
	19	143	1,386	449
			1,286	
	18	120	2,487	792
			4,530	
			2,784	
	19	100	8,876	1,456
			7,529	
B	19	95	>22,941	1,742
			>17,761	
			443	
	78	181	351	176
			507	
			907	
	116	143	740	383
			2,510	
			1,159	
	138	120	1,508	688
C	189	181	273	158
			275	
	227	143	544	345
			1,076	
	250	120	960	622

growth measurement under BL loading<sup>8)</sup> (see Fig. 3). When those stress cycles following these loading levels are applied, the crack tip seems to have propagated out of the low- $da/dN$  regions. This is the reason for the reduced retardation effect of BL10<sup>5</sup> when compared with BL10<sup>4</sup>.



**Table 4** Computed fatigue crack propagation lives,  $N_p$ , for VA tests ( $\times 10^3$ )

Series Name	Test No.	$\sigma_{\min}$ (MPa)	$\sigma_{\max}$ (MPa)	$\Delta\sigma_{RMC}$ (MPa)	$N$ by experiments	$N_p$ by Closure Analysis	$N_p$ by LEFM Analysis	$N_p$ by Equivalent CA Analysis
$\beta$ 1L	$\beta$ 1L-120	20	166	120	1,621	816	676	789
	$\beta$ 1L-110	20	154	110	2,870	1,080	908	1,052
					2,752			
					6,027			
	$\beta$ 1L-95	20	135	95	7,422	1,818	1,566	1,740
					>40,480			
	$\beta$ 1L-90	20	129	90	>31,300	2,200	1,911	2,115
	$\beta$ 1L-85	20	123	85	>31,790	2,706	2,376	2,623
$\beta$ 3L	$\beta$ 3L-120	27	316	120	1,705	892	632	776
	$\beta$ 3L-108	27	288	108	3,240	1,230	893	1,101
	$\beta$ 3L-95	19	247	95	2,872	1,942	1,424	1,728
	$\beta$ 3L-93	19	244	93	3,776	2,028	1,491	1,864
	$\beta$ 3L-82	19	217	82	6,453	3,127	2,349	3,006
	$\beta$ 3L-80	20	213	80	15,569	3,417	2,578	3,325
	$\beta$ 3L-75	20	201	75	12,790	4,216	3,264	4,458
	$\beta$ 3L-70	20	188	70	20,396	7,363	4,228	6,720
					24,269			
	$\beta$ 3L-65	20	177	65	46,629	13,357	5,629	Infinite
$\beta$ 3H	$\beta$ 3H-95	32	260	95	2,493	1,527	1,424	1,600
	$\beta$ 3H-79	65	256	79	2,347	2,933	2,678	3,094
	$\beta$ 3H-71	89	260	71	5,401	4,286	4,042	4,460
	$\beta$ 3H-52	134	258	52	21,781	16,368	15,295	Infinite

## (2) Crack initiation life

The crack initiation lives,  $N_i$ , calculated by  $N_i = N - N_p$ , are shown in Fig. 15. In Fig. 16,  $N_i$  are normalized by the test data,  $N$ . It can be seen that for the same block size, both  $N_i$  and normalized  $N_i$  increased with the decrease of equivalent stress range. The effect of block size at each stress range level is not large, except that the test of BL10<sup>5</sup> at  $\Delta\sigma = 133\text{MPa}$  showed an infinite  $N_i$ .

## 6. ANALYTICAL RESULTS FOR VA LOADING

The analytical results under CA and VA loading are shown in Tables 3 and 4. For VA tests, besides the analysis by the established model, the linear elastic fracture mechanics analysis and the analysis considering closure effect under the equivalent CA loading are also carried out. The three types of analyses are termed as Closure Analysis, LEFM Analysis and Equivalent CA Analysis, respectively. The stress range of an equivalent CA loading is defined as  $\Delta\sigma_{RMC}$  of the corresponding VA loading, which is the root-mean-cube value of all stress cycles in a loading block. The minimum stress and maximum stress are set to be the same as those of VA loading for constant-minimum-stress and constant-maximum-stress cases. For example, the equivalent

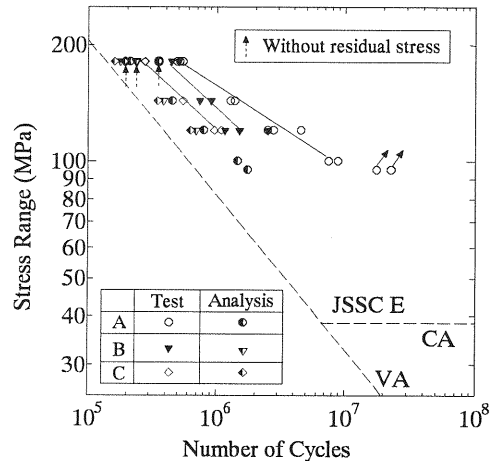


**Fig. 17** Closure Analysis for CA tests

CA loading of  $\beta$  1L-120 is  $\sigma_{\min} = 20\text{MPa}/\sigma_{\max} = 140\text{MPa}$ , and that for  $\beta$  3H-95 is  $\sigma_{\min} = 165\text{MPa}/\sigma_{\max} = 260\text{MPa}$ . For the purpose of comparison, the number of cycles in each computation step is set to be one.

### (1) Results of Closure Analysis for CA tests

The results of Closure Analysis for CA tests are shown in Fig. 17. The test data are also plotted for comparison. The solid lines are obtained through

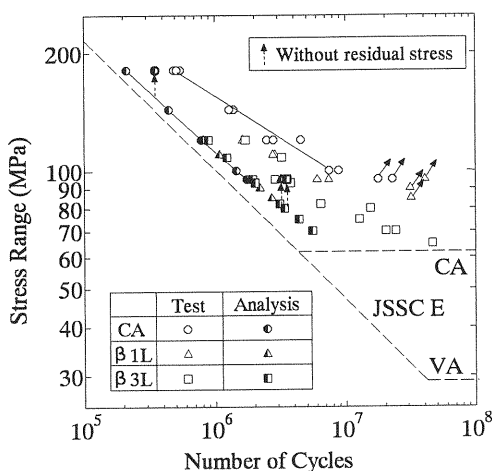


Fig. 18 Closure Analysis for constant-minimum-stress tests

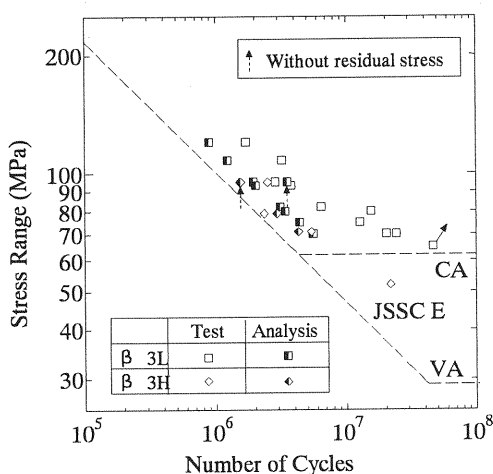


Fig. 19 Closure Analysis for  $\beta 3$  loading

least square method for the test data. It can be seen that the stress ratio effect, observed from the test data, is predicted by the analysis. However, the predicted stress ratio effect seems to be less.

The results of the prediction at  $\Delta\sigma = 181\text{MPa}$  without considering the residual stress are marked by arrows. It can be seen that by neglecting the residual stress, the predicted stress ratio effect becomes closer to that of the test data. All of the points move right, and the amount of the movement seems to be larger for the low-stress-ratio loading condition. For series A or B, the consideration of the residual stress actually raises the stress ratio level and therefore diminishes the crack closure effect. As a result, the fatigue crack propagation lives are shortened. For series C, the loading condition with the highest stress ratio, the consideration of the residual stress does not

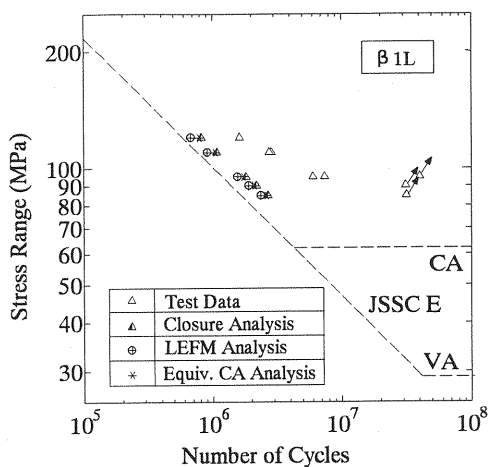


Fig. 20 Analytical results for  $\beta 1L$

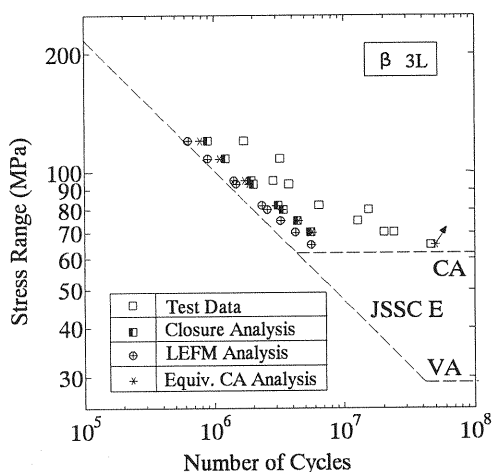


Fig. 21 Analytical results for  $\beta 3L$

cause significant change on the predicted fatigue crack propagation life. This is due to the fact that the crack closure effect is rather little even if there is no residual stress.

## (2) Results of Closure Analysis for constant-minimum-stress tests

The results of Closure Analysis for constant-minimum-stress tests are shown in Fig. 18. Test results are also plotted for comparison. The two straight lines show the mean  $S-N$  curve for CA test data and the corresponding mean  $S-N_p$  curve for analytical results.

When the test data are plotted by the equivalent stress range, both  $\beta 1L$  and  $\beta 3L$  show shorter fatigue life than that estimated by linearly extending the CA  $S-N$  curve. However, the analytical result

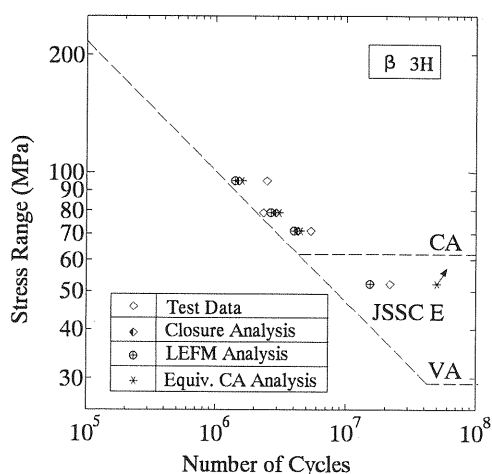


Fig. 22 Analytical results for  $\beta 3H$

does not show such trend. The predicted fatigue lives under VA loading deviate little from those under CA loading. In other words, the shortened experimental VA fatigue life compared to CA tests may be due to the relatively short crack initiation life under VA loading. Increasing the stress level will decrease the percentage of crack initiation life in total fatigue life. The VA loading, especially  $\beta 3L$  loading, contains a large number of high stress cycles. This contributes to the shortened fatigue crack initiation life.

Another conclusion that can be drawn from the figure is that load interaction effect in both  $\beta 1L$  and  $\beta 3L$  loading is negligibly small. This will be further discussed in the following.

### (3) Results of Closure Analysis for $\beta 3$ loading

Figure 19 shows the results of Closure Analysis for  $\beta 3L$  and  $\beta 3H$  loading. The points of the prediction at  $\Delta\sigma = 95\text{MPa}$  without considering welding residual stress are marked by arrows. It should be noted that for  $\beta 3H$ , the points with and without residual stress coincide with each other. This seems to be caused by the same reason as stated for series C in Fig. 17. The approximate stress ratio<sup>9</sup> for  $\beta 3H$  is 0.729, at which level the closure effect is rather little even if there is no residual stress. For  $\beta 3L$ , the approximate stress ratio is 0.325. The consideration of welding residual stress makes this level rise up and therefore differs much from the case without residual stress.

### (4) Analytical results of $\beta 1L$ , $\beta 3L$ and $\beta 3H$

The predicted results under  $\beta 1L$ ,  $\beta 3L$  and  $\beta 3H$  loading by Closure Analysis, LEFM Analysis and

Equivalent CA Analysis are shown in Figs. 20, 21 and 22. The phenomena observed from the figures are summarized as follows.

- Equivalent CA Analysis gives two points with infinite fatigue lives, one is for  $\beta 3L$  and the other one is for  $\beta 3H$ . The two points are plotted at  $N = 5 \times 10^7$ . This is due to the fact that the effective stress intensity factor ranges in these two cases are lower than the threshold level. In Closure Analysis, the large stress cycles propagate the crack. As a result, fatigue life becomes definite though the equivalent stress range is the same.
- Equivalent CA Analysis predicts almost the same fatigue life as Closure Analysis. This means that the load interaction effect in the current VA loading condition is rather little. In another words, the fatigue life under VA loading can be evaluated through the analysis on CA loading that has the same level of equivalent stress range. This observation is the same as that obtained through the fatigue crack growth measurement<sup>9</sup>.
- The fact that load interaction effect is little does not certainly lead to the conclusion that crack closure effect is little, too. For  $\beta 1L$  and  $\beta 3L$  loading, LEFM Analysis predicts slightly shorter  $N_p$  compared to Closure Analysis and Equivalent CA Analysis. This is because the crack closure effect, which is not negligible, is not taken into account in LEFM Analysis. For  $\beta 3H$  loading, the results from LEFM Analysis become close to those from the other two types of analyses due to the increased mean stress level that weakens the crack closure effect.

## 7. SUMMARY

The present study aims at clarifying the influence of load interaction on the fatigue behavior of highway bridge components under service loading condition. Fatigue crack growth analysis is carried out on non-load-carrying cruciform joints under POL, BL and VA loading, and compared with that under CA loading. The main findings are summarized as follows.

### POL loading:

- The damage effect of periodic overloads to fatigue crack propagation was dominant when the overload interval was 10. On the other hand, the overloads increased the fatigue crack propagation life if they were spaced at  $10^3$  or farther apart. The overload interval that was

most beneficial in extending the fatigue crack propagation life was  $10^4$  for such loading condition.

2. For each overload interval, the fatigue crack propagation lives under three levels of stress range were almost the same, i.e., stress range had little effect on load interaction under such loading conditions.
3. For the same overload interval, increasing stress range made the proportion of fatigue crack initiation life in total fatigue life decrease. For the same stress range, the proportion of fatigue crack initiation life in total fatigue life seems to increase with the overload interval.

#### BL loading:

4. Fatigue crack growth retardation occurred in the tests under those block sizes larger than  $10^2$ . The most beneficial block size in extending the fatigue crack propagation life is  $10^4$ .
5. For the same block size, the proportion of fatigue crack initiation life in total fatigue life increased with the decrease of the equivalent stress range of loading spectrum.

#### VA loading:

6. The test data under VA loading were found to be lower than those under the corresponding CA loading, when the data are plotted with equivalent constant stress ranges. This may be due to the influence of crack initiation stage. The predicted fatigue crack propagation life shows little difference between VA and CA loading.
7. Load interaction effect in the current loading conditions was found to be small.
8. For the loading spectrum with constant minimum stress, crack closure effect was not negligible. On the other hand, for that with constant maximum stress, crack closure effect became negligibly small due to higher mean stress level.

In almost all experiments, crack closure effect exists. Neglecting this effect in fatigue design may lead to conservative evaluation on fatigue life.

Load interaction effect was significant for POL and BL loading. For VA loading, this effect was rather small.

**ACKNOWLEDGEMENT:** This study was carried out under the Grant-in-Aid for Scientific Research from the Japanese Ministry of Education, Science, Sports and Culture.

#### **REFERENCES**

- 1) British Standard Institution, Steel, Concrete and Composite Bridges, *Code of Practice for Fatigue*, British Standard 5400: Part 10, 1980.
- 2) European Convention for Constructional Steelwork (ECCS), Technical Committee 6 - Fatigue, *Recommendations for the Fatigue Design of Steel Structures*, 1985.
- 3) American Association of State Highway and Transportation Officials (AASHTO), *Standard Specifications for Highway Bridges*, Fourteenth version, 1989.
- 4) Japanese Society of Steel Construction (JSSC), *Fatigue Design Recommendations for Steel Structures*, Gihoudou, April, 1993 (in Japanese).
- 5) Melhem, H. G. and Klippstein, K. H.: *A study on variable amplitude load fatigue: Work-in Progress*, Research Report No. ST-6, University of Pittsburgh, Jan., 1990.
- 6) Cheng, X. H. and Yamada, K.: Fatigue crack growth rate measurement of structural steel under overload conditions, *Structural Eng./Earthquake Eng.*, Japan Society of Civil Engineers, Vol. 11, No. 1, pp. 45-52, April, 1994.
- 7) Yamada, K., Cao, Q., Okuhara, Y. and Cheng, X.: Fatigue crack growth behavior of various structural steel after single and periodic overload, *Structural Eng./Earthquake Eng.*, Japan Society of Civil Engineers, Vol. 15, No. 2, 191s-200s, July, 1998.
- 8) Yamada, K., Okado, N. and Cao, Q.: Fatigue crack growth behavior under periodic overload and variable amplitude block loading, *Journal of Structural Engineering*, Japan Society of Civil Engineers, Vol. 44A, pp. 1133-1140, Mar., 1998.
- 9) Yamada, K., Cao, Q. and Okado, N.: Fatigue crack growth behavior under variable amplitude loading, *Journal of Structural Engineering*, Vol. 45A, pp. 1211-1220, Japan Society of Civil Engineers, March, 1999 (in Japanese).
- 10) Yamada, K., Cao, Q. and Okado, N.: Fatigue crack growth measurements under spectrum loading, *Engineering Fracture Mechanics*, 2000. (to be published)
- 11) Cao, Q.: Fatigue evaluation for highway bridge components under variable amplitude loading, Doctoral Dissertation, Nagoya University, Nagoya, Japan, June, 1999.
- 12) Elber, W.: The significance of fatigue crack closure, *Damage Tolerance in Aircraft Structures*, ASTM STP 486, American Society for Testing and Materials, pp. 230-242, 1971.
- 13) Abtahi, A., Albrecht, P. and Irwin, G. R.: Fatigue of periodically overloaded stiffener detail, *Journal of Structural Division*, American Society of Civil Engineers, Vol. 102, No. ST11, pp. 2103-2119, Nov., 1976.
- 14) Albrecht, P. and Yamada, K.: Simulation of service fatigue loads for short-span highway bridges, *Service Fatigue Loads Monitoring, Simulation, and Analysis*, ASTM STP 671, American Society for Testing and Materials, pp. 255-277, 1979.
- 15) Kondo, A. and Yamada, K.: Fatigue tests of non-load carrying cruciform joint under variable amplitude loading, *Journal of Structural Engineering*, Japan Society of Civil Engineers, Vol. 43A, pp. 1171-1181, Mar., 1997 (in Japanese).
- 16) Yamada, K. and Hirt, M. A.: Fatigue crack propagation from fillet weld toes, *Journal of the Structural Division*,

- American Society of Civil Engineers, Vol. 108, No. ST7, July, 1982.
- 17) Yamada, K. and Cheng, X. H.: Fatigue life analysis on welded joints under various spectrum loadings, *Journal of Structural Engineering*, Japan Society of Civil Engineers, Vol. 39A, Mar., 1993.
  - 18) Albrecht, P. and Yamada, K.: Rapid calculation of stress intensity factors, *Journal of the Structural Division*, American Society of Civil Engineers, Vol. 103, No. ST2, pp. 377-389, Feb., 1977.
  - 19) Newman, J. C., Jr.: Application of a closure model to predict crack growth in three engine disc materials, *International Journal of Fracture*, Vol. 80, pp. 193-218, 1996.
  - 20) Ibso, J. B.: Fatigue life prediction of welded joints based on fracture mechanics and crack closure, Doctoral Dissertation, Department of Structural Engineering, Technical University of Denmark, Lyngby, Denmark, Oct., 1996.
  - 21) Maddox, S. J.: *Fatigue Strength of Welded Structures*, Second edition, Woodhead Publishing Ltd., England, 1991.

(Received September 30, 1999)